Black Sea Journal of Engineering and Science
doi: 10.34248/bsengineering.1749453

Open Access Journal
e-ISSN: 2619 – 8991

Research Article
Volume 8 - Issue 6: 1802-1811 / November 2025

OPTIMIZING REFLOW SOLDERING OVEN TEMPERATURE CONTROL: A MATHEMATICAL APPROACH WITH FIRST-ORDER MODELLING AND PI CONTROLLER DESIGN

Cağfer YANARATEŞ[1], Aytaç ALTAN[2]*

[1]*Gümüşhane University, Department of Electrical and Energy, Kelkit Aydın Doğan Vocational School, 29600, Gümüşhane, Türkiye*
[2]*Zonguldak Bülent Ecevit University, Department of Electrical Electronics Engineering, 67100, Zonguldak, Türkiye*

Abstract: This paper presents a comprehensive analysis of the identification and control of a reflow soldering oven, with the primary goal of developing a Proportional-Integral (PI) controller to ensure precise temperature regulation and high-quality solder joints in circuit board manufacturing. The study begins by examining the generic thermal profile of a reflow soldering oven, offering insights into its temperature dynamics and control requirements. A mathematical model of the oven is derived using a first-order transfer function with transport delay, based on system response analysis. This model serves as the basis for designing and tuning the PI controller. The design process involves a systematic approach, including model validation and performance analysis under various operating conditions. The optimization of temperature control focuses on minimizing overshoot, compensating for steady-state errors, and ensuring robust responses to disturbances. Comprehensive simulations are conducted to evaluate the system's performance and stability, taking into account potential disturbances, noise, and time delays. The effectiveness of the developed PI controller is validated through comparisons with a simple Proportional (P) controller, and its accuracy is verified using the pole placement method. The results demonstrate significant improvements in temperature control, highlighting the controller's ability to precisely maintain desired thermal profiles.

Keywords: Reflow soldering oven temperature control, First-order systems, PI controller tuning, Pole placement method, Transfer function modelling

***Corresponding author:** Zonguldak Bülent Ecevit University, Faculty of Engineering, Department of Electrical Electronics Engineering, 67100, Zonguldak, Türkiye
E mail: aytacaltan@beun.edu.tr (A. ALTAN)
Cağfer YANARATEŞ https://orcid.org/0000-0003-0661-0654
Aytaç ALTAN https://orcid.org/0000-0001-7923-4528

Received: July 23, 2025
Accepted: September 23, 2025
Published: November 15, 2025

Cite as: Yanarateş C, Altan A. 2025. Optimizing reflow soldering oven temperature control: A mathematical approach with first-order modelling and PI controller design. BSJ Eng Sci, 8(6): 1802-1811.

1. Introduction

Mathematical modelling serves as a cornerstone for the analysis and design of complex systems with uncertainties and unavoidable parameter variations, playing a critical role in modern engineering (Davidson and Ringwood, 2017; Deb et al., 2020; Chen et al., 2021). With advances in technology, the widespread adoption of real-time interface (RTI) and hardware-in-the-loop (HIL) systems has further emphasized the importance of robust mathematical modelling techniques (Zia et al., 2022; Mihalič et al., 2022; Bhayo et al., 2023; Yanarateş et al., 2024). Accurate and reliable models are essential for the development of sophisticated control strategies to ensure system stability, performance and efficiency, especially for black-box and white-box systems where prior information may be limited (Hannan et al., 2018; Lashab et al., 2018; Birs et al., 2019).

To enable optimal design and control strategies, a deep understanding of mathematical modelling tools is crucial. These tools allow the simulation of system behaviour under varying conditions, providing a basis for effective system analysis and design (Minchala-Avila et al., 2015; Silvas et al., 2016). In this context, this study focuses on the design of a proportional-integral (PI) controller for a reflow soldering oven, demonstrating the critical role and benefits of mathematical modelling in engineering applications (Borase et al., 2021; Jamil et al., 2022; Chen, 2023).

Reflow soldering ovens are essential in the manufacture of electronic circuit boards, where precise temperature control is critical for the production of high-quality solder joints (Cheng et al., 2017; Said et al., 2023). The PI controller design process for such ovens requires a comprehensive understanding of the system dynamics, which can be effectively captured by various mathematical modelling techniques. Table 1 outlines four basic modelling approaches commonly used in control systems, highlighting their respective advantages and limitations (Hou et al., 2017; Karamanakos et al., 2020; Li and Peissig, 2020).

Reflow soldering ovens play a key role in modern electronics manufacturing by providing consistent heating and cooling during the soldering process. Their temperature-controlled zones allow precise thermal management to accommodate varying solder paste

properties and component thermal tolerances. By maintaining optimal thermal profiles, these ovens increase production yields, reduce defects and improve overall product reliability, making them essential for the assembly of complex electronic devices.

Incorporating HIL testing into reflow soldering systems further enhances their functionality. HIL enables real-time emulation of physical systems, making it easier to develop and test control algorithms without exposing the actual hardware. This approach minimizes prototyping costs, shortens development cycles and improves safety by simulating operating scenarios under controlled conditions. In process control applications such as reflow soldering, HIL systems support better performance tuning, increased robustness and more thorough system validation, ultimately leading to higher product quality and reliability in industrial manufacturing.

This paper presents a detailed analysis and verification of a PI controller using a first-order transfer function with transport delay. This modelling approach is particularly advantageous due to its suitability for efficient time and frequency domain analysis. It provides straightforward methods for stability evaluation and controller parameter tuning, making it highly effective for compensator design. By transforming differential equations into algebraic equations, this method provides a reliable framework for analyzing and modelling control systems. Key concepts such as poles, zeros, stability and sensitivity can be thoroughly investigated through the transfer function. Although limited to linear systems, transfer functions offer numerous analytical and design advantages in a simplified and practical form. They continue to play an important role in both academic research and industrial applications, serving as a fundamental tool in the analysis and design of control systems.

The remainder of the paper is structured as follows: Section 2 presents the ramp response of the first-order system, detailing all stages of the process, including the response characteristics of the time-domain analysis, and introduces the impact of transport delay in first-order systems. A comprehensive analysis of the thermal profile of the reflow soldering oven is also provided, followed by the mathematical modelling of the proposed system. The controller design process, including P control, PI control, and the performance evaluation of the controller designed using the pole placement method, is discussed in detail. Section 3 presents the results and discussion. Finally, the study concludes with the findings summarized in Section 4.

Table 1. The most used mathematical models

Mathematical Model	Advantages	Disadvantages
State-Space Model (Chen et al., 2021; Tsui, 2022)	•Comprehensive depiction •Detailed representation •Appropriate to multi-input-multi-output (MIMO) systems •Ease of use with modern control architecture	•Needs in-depth understanding of the system •Complexity for large systems
Transfer Function (Nise, 2020; Åström and Murray. 2021)	•Simple design and direct representation •Widespread application •Facilitates time and frequency domain analyses	•Restricted to single-input-single-output (SISO) systems •Potential information loss on internal state
Block Diagram (Nise, 2020; Susanto et al., 2021)	•Visual display •Convenient for understanding the system structure intuitively •Enables modular design easier and simpler	•Potential burdensome for complex systems •Not suitable enough for comprehensive investigation and rigorous analysis
Linear Differential Equations (Nise, 2020; Gu et al., 2021)	•A profound link to physical laws •Easily identified and simply derivation •Fitting for simple systems	•Challenging to resolve for intricate systems •Less intuitive for controller design

2. Materials and Methods

This section is structured as follows: First, the ramp response of the first-order system is analyzed in detail, including all stages of the process, time-domain response characteristics and the effect of transport delay. Next, a comprehensive analysis of the thermal profile of the reflow oven is presented, focusing on its temperature dynamics and operational behaviour. This is followed by the mathematical modelling of the proposed system, which provides a basic framework for control system design. Finally, the controller design process is discussed, covering P and PI control methods, along with a performance evaluation of the designed controllers using the pole placement method.

2.1. Ramp Response of the First-Order Systems and the Impact of Transport Delay

This section details the steps involved in analyzing the ramp response of a first-order system. The process includes the representation of the system's transfer function, the application of the Laplace transform, and the examination of key time-domain characteristics, such as steady-state error, overshoot, and undershoot. These steps are summarized in Table 2. The mathematical transformations discussed in this study act as a bridge between the theoretical behaviour of a system and its practical applications. For example, the Laplace transform simplifies the analysis of differential equations by converting them into more manageable algebraic

expressions. Considering a first-order system with a transfer function $G(s) = \frac{K}{\tau s+1}$, the application of a unit step input $R(s) = \frac{1}{s}$ results in the following transformed output:

$$Y(s) = G(s)R(s) = \frac{K}{\tau s+1}\frac{1}{s} = \frac{K}{\tau}\left(\frac{1}{s} - \frac{1}{s+\tau^{-1}}\right) \quad (1)$$

By applying the inverse Laplace transform, the time domain response of the system is obtained as

$$y(t) = \frac{K}{\tau}(1 - e^{-\frac{t}{\tau}}) \quad (2)$$

where K is the system gain and τ is the time constant. This expression illustrates the exponential behaviour and settling characteristics of the system in response to a step input, highlighting its transient dynamics and steady state behaviour. Such detailed commentary aims to provide the reader with a clearer understanding of the underlying physical processes being modelled, while emphasizing how theoretical constructs such as system gain and time constant manifest themselves in real-world applications, such as the impact of transport delays on system performance and stability.

In practical applications, the system gain and time constant play a critical role, as they directly impact the behaviour and overall performance of a system in real-world conditions. System gain influences the magnitude of the output response relative to a given input, thereby affecting the system's sensitivity. In industrial control systems, achieving the right balance of system gain is crucial for ensuring reliable and stable operation and preventing excessive oscillations.

Table 2. The first-order system ramp response

Step	Description
Transfer Function	The transfer function of a first-order system is given by $G(s) = \frac{K}{\tau s+1}$, where K is the system gain and τ is the time constant.
Input (Ramp Function)	The Laplace transform of a ramp input ($r(t) = t$) is $R(s) = \frac{1}{s^2}$
Output (Laplace Domain)	The output in the Laplace domain is $Y(s) = G(s)R(s) = \frac{K}{\tau s+1} \cdot \frac{1}{s^2} = \frac{K}{(\tau s+1)s^2}$
Partial Fraction Decomposition	Decompose $Y(s)$ into partial fractions: $Y(s) = \frac{K}{(\tau s+1)s^2} = \frac{A}{s} + \frac{B}{s^2} + \frac{C}{\tau s+1}$ Solving for A, B, and C gives $Y(s) = \frac{K}{\tau}\frac{1}{s} - \frac{K}{\tau^2}\frac{1}{s^2} + \frac{K}{\tau^2}\frac{1}{\tau s+1}$
Inverse Laplace Transform	Apply the inverse Laplace transform to find the time-domain response: $y(t) = \mathcal{L}^{-1}\left(\frac{K}{\tau}\frac{1}{s} - \frac{K}{\tau^2}\frac{1}{s^2} + \frac{K}{\tau^2}\frac{1}{\tau s+1}\right) = \frac{K}{\tau}t - \frac{K}{\tau^2}t + \frac{K}{\tau^2}(1 - e^{-t/\tau})$
Simplified Time Response	Simplify the time-domain response to: $y(t) = Kt - \frac{K}{\tau}(t - \tau + \tau e^{-t/\tau})$ $y(t) = Kt - \frac{K}{\tau}t + K(1 - e^{-t/\tau})$
Steady-State Error	The steady-state error e_{ss} is the difference between the input and output as $t \to \infty$ For a ramp input, $e_{ss} = \lim_{t\to\infty}(r(t) - y(t))$ $e_{ss} = \lim_{t\to\infty}\left(t - \left(Kt - \frac{K}{\tau}t + K\left(1 - e^{-t/\tau}\right)\right)\right) = \infty$
Overshoot Undershoot	For a first-order system, there is no overshoot in the ramp response. Similarly, there is no undershoot in the ramp response of a first-order system.

Rise Time (T_r)	Settling Time (T_s)	Time Constant (τ)
The time it takes for the response to go from 0 *to* 63.2% of its final value.	The time it takes for the response to remain within a certain percentage. It is usually $2\% - 5\%$ of the final value.	The time it takes for the system's response to reach $\cong$ 63.2% of its final value.

Similarly, the time constant determines how quickly a system responds to changes, affecting settling time and the ability to track desired setpoints or handle disturbances. In systems with significant transport delay, which is common in processes involving material handling, chemical reactions or thermal systems, response time is delayed. This can lead to sluggish performance or instability if not properly managed. Transport delay exacerbates the challenges associated with control by creating a lag between input changes and observable effects, making predictive control and compensatory strategies essential. Highlighting these aspects demonstrates the importance of understanding and managing these parameters for optimizing the performance of practical control systems and mitigating the adverse impacts of transport delay (Chen et al., 2021).

A first-order system's closed-loop feedback is likely to have a transport delay, often referred to as a time delay. This can cause the system to overshoot. As well as causing the system to respond more slowly to input changes, transport delays can also produce phase lag.

A first-order system with a transport delay of T_d can have the following representation for its transfer function:

$$G(s) = \frac{Ke^{-T_d s}}{\tau s + 1} \quad (3)$$

The system has additional phase lag because of the transport delay $e^{-T_d s}$. This translates as the system's output being T_d seconds slower than its input in the time

domain. This delay has the potential to cause oscillatory behaviour and overshoot by destabilising the system or reducing its phase margin. For a closed-loop system with feedback, the overall transfer function with transport delay is:

$$T(s) = \frac{G(s)}{1 + G(s)H(s)} = \frac{Ke^{-T_d s}}{(\tau s + 1) + Ke^{-T_d s}} \quad (4)$$

where $H(s)$ is the feedback transfer function, typically taken as 1 for unity feedback.

The impact of transport delay on the operation of a reflow soldering oven, where precise temperature control is essential for achieving optimal soldering quality, serves as an example of its influence on real-world control systems. Transport delay is the time lag between a controller's action and the system's observable response. This delay is particularly significant during rapid temperature changes. In a reflow soldering oven, for example, an unexpected delay in the heating element's response can lead to temperature overshoot or prolonged exposure to high heat. This can result in defects such as weakened solder joints or component overheating. Accurately quantifying and compensating for transport delay enables control systems to achieve smoother and more precise transitions through critical temperature zones, thereby enhancing reliability and product quality. This example highlights the importance of effectively managing transport delay in practical control applications.

2.2. Reflow Soldering Oven Thermal Profile

Reflow soldering is a widely used technique for attaching electronic components to a PCB both mechanically and electrically. The process involves preheating the PCB, components and solder paste initially, before carefully melting the solder to form reliable connections without scorching or damaging the components. The aim is to create strong, defect-free solder joints. Figure 1 illustrates the thermal profile of a reflow soldering oven, outlining the controlled temperature stages essential for achieving this outcome.

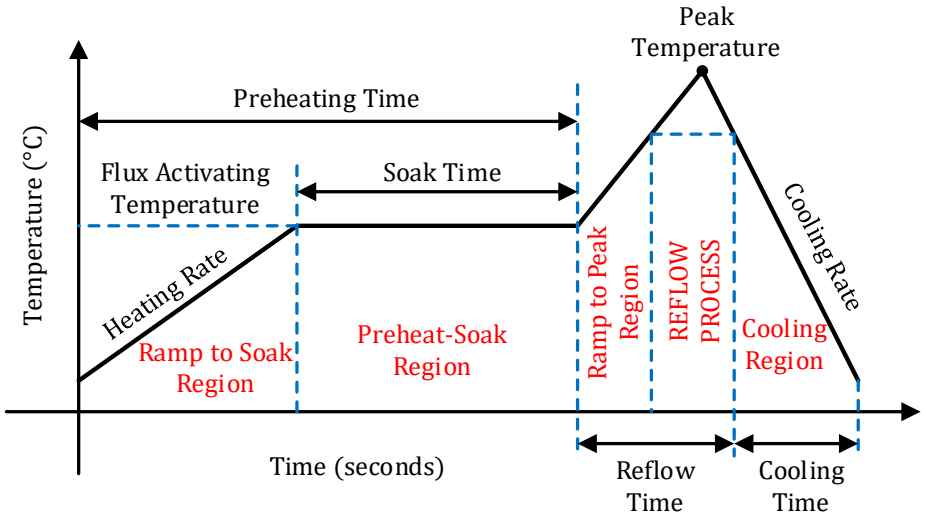

Figure 1. Reflow soldering oven thermal profile.

The entire process can be evaluated as comprising four different zones, summarized in Table 3 along with their effects. The first step in the reflow process is preheating. During this phase, the entire board assembly rises towards the desired soak or dwell temperature. The primary objective of the preheat phase is to reach a soak or pre-reflow temperature for the entire assembly in a safe and reliable manner. In the recirculating (thermal soak) zone, the solder paste's volatiles are removed and the fluxes are activated to reduce oxide on the component leads and pads. The temperature is at its maximum in the reflow zone. Peak temperature is a crucial factor to consider as it represents the maximum temperature permitted during the procedure. The final zone is a cooling zone, which hardens the solder junctions and gradually cools the processed board. Proper cooling prevents excessive intermetallic development and component thermal stress.

2.3. Mathematical Modelling of the System

The plant needs to be modelled to develop and execute a reliable (efficient and robust) temperature control system. In this sense, the goal is to undertake an attempt to create a more intelligent control algorithm and to explain the control system's resulting behaviour. Based on the reflow soldering oven's observed response, a model for its thermal behaviour is created. Once the model is created appropriately, system behaviors will be analyzed in the simulation environment, and a reliable control unit will be developed to apply to the real system. In the thermal profile shown in Figure 1, the system input follows a finite-duration ramp rather than an infinite ramp. Specifically, the temperature increases linearly during the Ramp to Soak Region until the flux activating temperature is reached, after which the input remains constant during the Preheat–Soak Region, and later changes again in the Ramp to Peak Region. This behavior differs fundamentally from the case of a

continuous, unbounded ramp input. For a finite-duration ramp input, the steady-state error, overshoot, and undershoot characteristics differ from those of an infinite ramp input:

• **Steady-state error:** For $K \neq 1$ in a first-order plant, the tracking error increases linearly during the ramp and, after the ramp ends, decays exponentially to a constant value set by the system gain and final reference.

• **Overshoot:** Absent in an open-loop first-order ramp response, but may appear in closed-loop systems (e.g., temperature control in a reflow oven) after the ramp due to controller dynamics and thermal inertia.

• **Undershoot:** Not present in open-loop operation, but may occur in closed-loop systems if oscillatory settling follows overshoot.

The finite-duration ramp input can be mathematically described as:

$$r(t) = \begin{cases} at, & 0 \leq t < T_r \\ aT_r, & t \geq T_r \end{cases} \quad (5)$$

where a is the slope of the ramp and T_r is the ramp duration.

For a first-order plant $G(s) = \frac{K}{\tau s+1}$, the output is:

$$y(t) = \begin{cases} aKt - aK\tau + aK\tau e^{-t/\tau}, 0 \leq t < T_r \\ KaT_r + (y(T_r^-) - KaT_r)e^{-(t-T_r)/\tau}, t \geq T_r \end{cases} \quad (6)$$

where:

$$(y(T_r^-) = aKT_r - aK\tau + aK\tau e^{-T_r)/\tau}. \quad (7)$$

The corresponding tracking error is:

$$e(t) = \begin{cases} (1-K)at + aK\tau(1 - e^{-t/\tau}), 0 \leq t < T_r \\ aT_r(1-K) - (y(T_r^-) - KaT_r)e^{-(t-T_r)/\tau}, t \geq T_r \end{cases} \quad (8)$$

This model shows that for a finite-duration ramp, the error increases linearly during the ramp phase but settles to a constant value after the ramp ends, in contrast to the infinite ramp case where the error grows unbounded as $t \to \infty$.

The plant parameters were identified from simulation-based ramp response data. The reference input was a finite-duration ramp profile with a slope of $a = 2.5$ °C/s and a duration of $T_r = 20\ s$. These values were selected according to widely accepted reflow soldering process guidelines in Table 3. The system was modeled as a first-order-plus-dead-time (FOPDT) transfer function to characterize its dynamic parameters:

$$G(s) = \frac{K}{\tau s + 1} e^{-T_d s} \quad (9)$$

where K is the plant gain, τ is the time constant, and T_d is the time delay.

The parameters were estimated using the nonlinear least-squares curve fitting method (NLSCF). Initial estimates were obtained from the process reaction curve method and refined by minimizing the mean squared error. The time delay was determined from the time difference between the ramp onset and the first observable response in the simulation. The final identified parameters were $K = 1.92$, $\tau = 15.8\ s$, and $T_d = 0.187\ s$.

The model achieved a normalized root mean square error (NRMSE) fit of 96.3% to the simulated data. The 95% confidence intervals for the parameters, derived from the parameter covariance matrix were $K \in [1.89,1.95]$, $\tau \in [15.2,16.4]\ s$, $T_d \in [0.182,0.192]\ s$.

Examining the provided ramp response data in literature, the steady-state oven temperature is selected as 120 °C, and the ambient temperature (initial oven temperature) 25 °C. Given that the output is ΔT and the input is equal to 1 (100 percent duty cycle), the system's DC gain K is roughly 95 °C. According to the definition of time constant, which is the amount of time it takes for a system's response to reach 63% of its total change, the proposed system's time constant is aimed to be approximately 220 seconds. Based on the determined values, the following is an estimation of the thermal dynamics model for the suggested reflow oven:

$$P(s) = \frac{\Delta T(s)}{D(s)} = \frac{95}{220s + 1} \quad (10)$$

The results obtained from the simulation of the derived transfer function in Equation (10) are investigated and a transport delay of 187 milliseconds is added to it. Thus, the addition of transport delay resulted in the following new transfer function:

$$P(s) = \frac{\Delta T(s)}{D(s)} = \frac{95e^{-0.187s}}{220s + 1} \quad (11)$$

Figure 2 shows the resulting waveforms from simulating the model without a controller. This enables us to illustrate more clearly how well the derived model fits the experimental data.

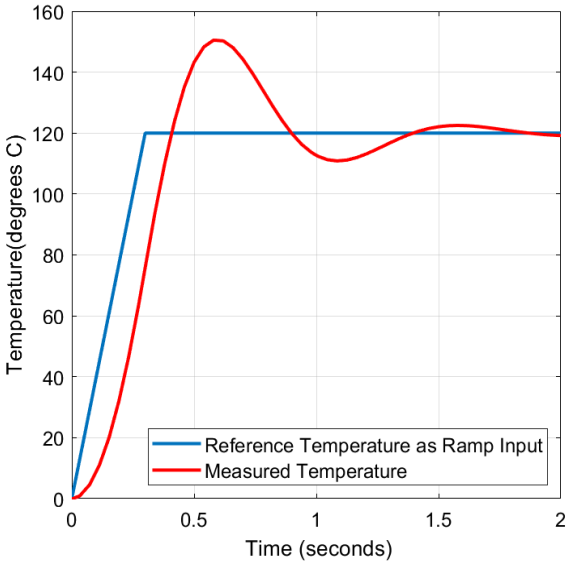

Figure 2. Resulting waveform of the derived transfer function simulation.

Table 3. The reflow soldering oven thermal zones

Zone	Effect	General Setting Values
Preheating Zone	Volatilization of solvent	Heating rate: < 2.5 ℃/Sec. Time: 2 to 4 $Minute\ Max$.
Recirculating Zone (Thermal Soak)	Flux action and plate	Recommended Soak Time: 60 to 90 Sec. (120 $Sec. Max$.)
Reflow Zone	temperature balance	Recommended Reflow Time: 30 to 50 Sec. (70 $Sec. Max$.)
Cooling Zone	Melting of solder paste	Cooling Time: 180 $Sec. Minimum$

The application of the reference value as ramp input highlights the significance of temperature slope rate. The temperature slope rate or rise vs time is one of the crucial reflow process metrics, which is often measured in degrees Celsius per second, ℃/s. In the experimental setup utilised for system identification and, subsequently, modelling, the slope rate was selected as 0.6 ℃/s.

Benchmark comparisons with three alternative identification methods—the Ziegler–Nichols reaction curve method, the Cohen–Coon method, and the MATLAB procest function (FOPDT model)—were performed using the same simulation dataset to verify the accuracy of the system's mathematical model derived in Equation (11).

The performance of each identified model was evaluated using NRMSE, mean absolute error (MAE), and integral of squared error (ISE). Table 4 summarizes the benchmark results.

Table 4. Benchmark comparisons with three alternative identification methods

Method	NRMSE (%)	MAE (°C)	ISE
Proposed NLSCF	96.3	0.42	5.13
Ziegler–Nichols	91.4	0.87	12.68
Cohen–Coon	89.7	0.95	14.52
procest (FOPDT)	93.8	0.61	9.84

The proposed method achieved the highest fit accuracy and lowest error values among the tested approaches, confirming the suitability of the identified model for control design purposes.

2.4. Controller Design

This section presents the design and implementation of a PI temperature controller for a reflow soldering oven. A key focus is placed on how the controller gains influence the location of the closed-loop poles, which in turn guides the fine-tuning of these gains. The controller is designed to achieve the desired transient response characteristics, while ensuring minimal steady-state error. The resulting closed-loop system is analyzed in detail to evaluate its performance. Figure 3 illustrates the overall control structure in idealized form.

The process of tuning the parameters of both P and PI controllers plays a critical role in achieving optimal system performance. The primary objective is to determine the appropriate controller gains to strike a balance between a fast dynamic response, minimal overshoot and high steady-state accuracy. There are several techniques that can be employed to select the most suitable gain values based on the system's performance requirements.

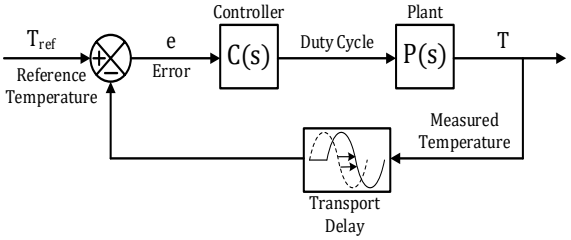

Figure 3. Idealized SISO model of closed-loop feedback with delay.

When tuning the P controller, the focus is on selecting a suitable proportional gain (K_p)that strikes a satisfactory balance between response speed and system stability. The gain is usually adjusted according to the desired response time and allowable overshoot. Initial values can be selected heuristically and then refined using methods such as loop shaping. In this method, the open-loop transfer function is modified to meet specific criteria such as bandwidth and phase margin.

In the case of the PI controller, adding an integral gain (K_i) improves the system's ability to eliminate steady-state error. Both K_p and K_i can be tuned using approaches such as the Ziegler-Nichols method, manual adjustment or pole placement techniques. The integral gain is carefully tuned to minimize steady-state error while maintaining system stability and preventing excessive oscillations.

Initially arbitrary K_p of 0.5, 1 and 1.5 are chosen. Figure 4 displays the temperature profiles that resulted after the implementation of these gains. With $C(s) = K_p$ and the previously defined $P(s)$, the result is the following closed-loop transfer function for this system.

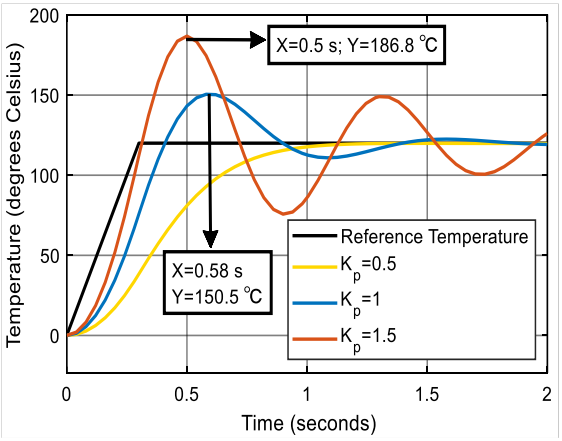

Figure 4. Reflow soldering oven temperature under P control.

$$G_{cl}(s) = \frac{C(s)P(s)}{1 + C(s)P(s)} = \frac{95e^{-0.187s}K_p}{220s + 1 + 95e^{-0.187s}K_p} \quad (12)$$

The resulting profiles that emerge demonstrate a correlation between the overshoot and the amount of steady-state error as compared to the supplied reference temperature of 120 °C.

A PI controller is generated by including a term in the controller that is proportional to the integral of the error. The form of this controller is $C(s) = K_p + K_i/s$. Using a controller such that, the feedback control system becomes type 1, and as a result, the steady-state error should be reduced. Accordingly, the system's closed-loop transfer function is produced as follows:

$$G_{cl}(s) = \frac{95e^{-0.187s}(K_p s + K_i)}{220s^2 + (1 + 95e^{-0.187s}K_p)s + 95e^{-0.187s}K_i} \quad (13)$$

In this stage, after choosing a proportional gain of 0.8, the impact of various integral values (K_i of 0.001, 0.02 and 0.05) on the system's performance was investigated. The resulting temperature profile and control effort for this model are given in Figure 5.

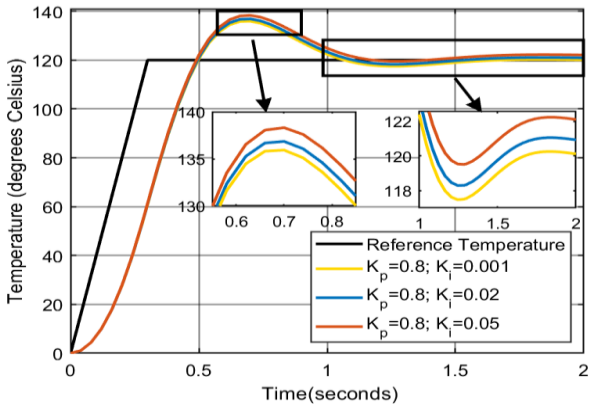

Figure 5. Reflow soldering oven temperature under PI control.

2.5. Controller Performance Assessment using Algebraic Pole Placement

Equation (13) shows that the closed-loop system with the PI controller is second order and has a zero. The presence of these zero means that the system does not match the canonical form displayed below.

$$G_{canon}(s) = \frac{{\omega_n}^2}{s^2 + 2\zeta\omega_n s + {\omega_n}^2} \quad (14)$$

The system is first regarded as though it has a canonical form, even though the zero is present. As a result, the original design will not accurately depict how the closed-loop system with zero behaves. Notwithstanding these drawbacks, this design will offer a solid foundation and prove to be a qualitatively beneficial evaluation in the controller's tuning. The relationships between control gains and desired closed-loop pole locations (as indicated by natural frequency ω_n, damped natural frequency ω_d, real part of the dominant pole σ and damping ratio ζ) can be obtained by matching the denominator of the closed-loop transfer function $G_{cl}(s)$ to the above canonical form in Equation (9) as follows:

$$2\zeta\omega_n = 2\sigma = \frac{(1 + 95e^{-0.187s}K_p)}{220} \quad (15)$$

$${\omega_n}^2 = \frac{95e^{-0.187s}K_i}{220} \quad (16)$$

Following that, control gains are selected to try and find closed-loop pole locations that satisfy the settling time t_s, peak time t_p, and maximum overshoot M_p parameters defined based on the reflow oven setting values given in Table 3.

To ensure that the settling time requirement is met, σ is confined with the following equation:

$$t_s \approx \frac{4}{\sigma} < 120 \;\Rightarrow\; \sigma > 0.0333 \quad (17)$$

By considering the peak time requirement, the following equation yields a constraint on ω_d:

$$t_p = \frac{\pi}{\omega_d} < 60 \;\Rightarrow\; \omega_d > \frac{\pi}{60} \approx 0.0524 \quad (18)$$

Lastly, ζ is constrained by the maximum percent overshoot criterion less than 20% is given by:

$$M_p = e^{-\zeta\pi/\sqrt{1-\zeta^2}} < 0.2 \;\Rightarrow\; \zeta > \sqrt{\frac{(ln0.2)^2}{\pi^2 + (ln0.2)^2}} \approx 0.456 \quad (19)$$

The closed-loop system will not be guaranteed to achieve the associated requirements even if the gains are selected to satisfy the three restrictions above because the system is not canonical (it has a zero) and the actual physical plant will differ from the theoretical model. Nevertheless, as will subsequently be shown, the correlations are still helpful in qualitatively guiding the setting of the control gains.

Each of these requirements will be mapped on the complex s-plane as indicated in Figure 6 to aid in their visualization. In particular, the real component of the poles is represented by σ, the imaginary part by ω_d, and the angle beta is mapped to ζ by the formula $\zeta = cos\beta$. Thus, $\beta < \cos^{-1}(0.4556) \approx 62.3^{\circ}$ is required and the regions shaded are the pole locations that meet each of the three criteria.

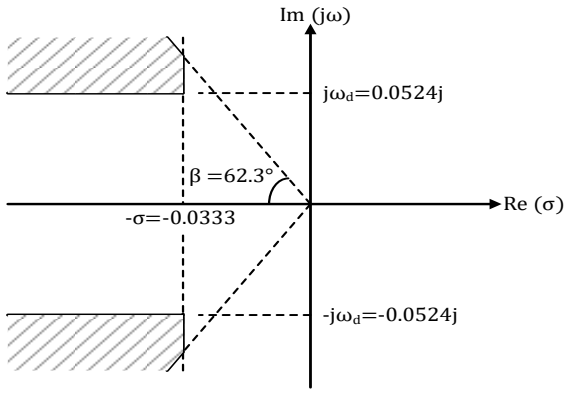

Figure 6. Targeted pole locations in s-plane.

Based on the requirements, these specifications are used to determine the closed-loop poles that equal $-0.16 \pm 0.0557j$. The primary disadvantage of choosing the poles to fulfil the requirements with a greater margin is that it usually requires more control effort to operate the system "faster" (smaller peak and settling times). Referring to the original closed-loop transfer function, the control gains K_p and K_i are determined as compatible with the pole locations shown in Figure 6, where $\sigma = 0.16$ and $\omega_d = 0.0557$. Accordingly, the gains of the PI controller are calculated as follows:

$$\frac{\left(1 + 95e^{-0.187s}K_p\right)}{220} = 2\sigma \;\Rightarrow\; K_p = 0.8807$$
$$\frac{95e^{-0.187s}K_i}{220} = {\omega_n}^2 = \sigma^2 + {\omega_d}^2 \Rightarrow\; K_i = 0.08 \quad (20)$$

The discrete implementation was carried out in MATLAB/Simulink using the identified FOPDT plant model ($K = 1.92$, $\tau = 15.8\,s$, $T_d = 0.187\,s$) and a PI controller with $K_p = 0.8807$ *and* $K_i = 0.08$, discretized via the Tustin method with a sampling period of $T_s = 0.1\,s$. The actuator was modeled with duty-cycle saturation limits of [0,1] and a rate limiter reflecting physical constraints, while the sensor block incorporated quantization and additive white noise to emulate measurement uncertainty. An anti-windup scheme based on integrator clamping was applied to prevent wind-up during actuator saturation.

Robustness to plant-parameter uncertainty was assessed by varying K, τ, and T_d independently by $\pm 20\%$. In the nominal finite-duration ramp case ($a = 2.5\,℃/s, T_r = 20\,s$), the closed-loop response was designed to achieve zero overshoot in the idealized model and exhibited a settling time of $73.1\,s$. However, in the discrete-time simulation with actuator limits, thermal inertia, and integral action, a small overshoot was observed, particularly for higher K_i values, due to the integrator continuing to supply control effort after the ramp ends. Under parameter variations, overshoot remained absent in most cases except $\tau + 20\%$, where it reached 0.46%. The settling time ranged from $62.9\,s$ ($K + 20\%$) to $88.5\,s$ ($K - 20\%$), corresponding to approximately -14% / $+21\%$ relative to nominal.

Frequency-domain robustness was verified using a first-order Padé approximation of the delay, yielding large stability margins across all cases ($GM \approx 136 - 214\,dB, PM \approx 84^{\circ} - 96^{\circ}$). These results confirm that the discrete controller is robust to sampling effects, actuator limits, measurement noise, and moderate uncertainties in K, τ, and T_d, thus complementing the pole-placement-based design with quantitative robustness validation.

3. Results and Discussion

To demonstrate the effectiveness of the suggested controller scheme, the designed PI controller has been verified and validated. This involved considering important factors such as complicated dynamics and nonlinearity, as well as the effects of the controller gains and system characteristics (e.g. temperature slope rate selection, undershoot, overshoot, and steady-state error). Figure 7 shows the trends of the modelled system at three different rise times (slope rates), which are among the most important parameters in reflow soldering oven temperature control.

When building heating systems for maximum efficiency, sensor consistency and accuracy are important considerations. As a system may use more data to enhance decision-making, the capacity of the sensors to correctly sense and record temperature levels reduces the time that the system needs to run. These sensors supply the raw data that the controller uses to regulate system operation for better performance. Therefore, it is of critical importance to evaluate the thermal profile of the reflow soldering oven over specified time intervals with varying slope rates.

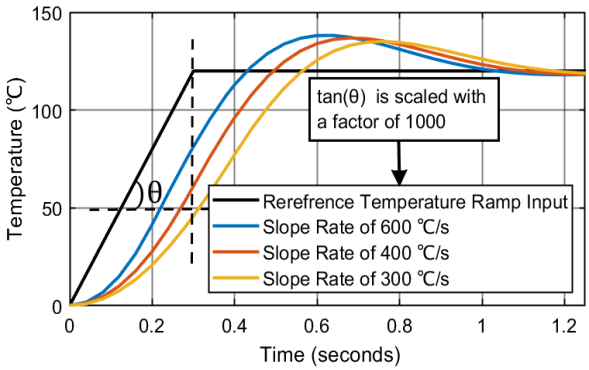

Figure 7. Response of the model at different slope rates.

Considering the general setting values given in Table 3, the temperature profiles shown in Figure 7 confirm the functionality and efficiency of the designed PI controller, which has a proportional gain of 0.8807 and an integral gain of 0.08. This is evident in terms of performance parameters such as accuracy, reliability, and speed.

4. Conclusion

This study involved designing a PI controller for temperature regulation in a reflow soldering oven using mathematical modelling as the core methodology. The modelling and simulation processes were carried out using MATLAB/Simulink, a powerful platform offering integrated tools for numerical computation and an interactive environment for modelling, analyzing and simulating systems. This approach allowed an accurate representation of the system to be developed without the need for detailed knowledge of the internal parameters of the physical system, demonstrating the flexibility and applicability of this modelling technique in control system design.

The system was modelled using the transfer function method, taking into account key real-world factors such as uncertainties, time delays and disturbances. Incorporating these elements into the model resulted in a control system that is robust, adaptive, and responsive

under varying operational conditions. The study also revealed that mathematical modelling facilitates the design of advanced control strategies and provides a valuable framework for detecting and analyzing system faults, offering a holistic approach to control and diagnostics.

A notable finding of the study was the critical role of the temperature sensor in system performance. The correct selection and precise placement of the sensor are essential components of any temperature control system and have a direct impact on time delay and, consequently, control accuracy. Proper positioning of the sensor ensures reliable and timely temperature measurements, enabling the control system to respond promptly to changes and maintain the desired thermal profile with minimal overshoot. This improves system stability and ensures consistent soldering quality in the manufacturing process.

Author Contributions

The percentages of the authors' contributions are presented below. All authors reviewed and approved the final version of the manuscript.

	C.Y.	A.A.
C	50	50
D	50	50
S	50	50
DCP	50	50
DAI	50	50
L	50	50
W	50	50
CR	50	50
SR	50	50

C=Concept, D= design, S= supervision, DCP= data collection and/or processing, DAI= data analysis and/or interpretation, L= literature search, W= writing, CR= critical review, SR= submission and revision.

Conflict of Interest

The authors declared that there is no conflict of interest.

Ethical Consideration

Ethics committee approval was not required for this study because of there was no study on animals or humans.

References

Åström KJ, Murray R. 2021. Feedback systems: an introduction for scientists and engineers. Princeton Univ Press, pp: 13.

Bhayo MA, Mirsaeidi S, Koondhar MA, Chandio S, Tunio MA, Allasi HL, Azız MJA, Idris NRN. 2023. An experimental hybrid control approach for wind turbine emulator. IEEE Access, 11: 58064-58077.

Birs I, Muresan C, Nascu I, Ionescu C. 2019. A survey of recent advances in fractional order control for time delay systems. IEEE Access, 7: 30951-30965.

Borase RP, Maghade DK, Sondkar SY, Pawar SN. 2021. A review of PID control, tuning methods and applications. Int J Dyn Control, 9: 818-827.

Chen Q, Li N, Feng W. 2021. Model predictive control optimization for rapid response and energy efficiency based on the state-space model of a radiant floor heating system. Energy Build, 238: 110832.

Chen R, Yuan Y, Thomson D. 2021. A review of mathematical modelling techniques for advanced rotorcraft configurations. Prog Aerosp Sci, 120: 100681.

Chen X. 2023. Temperature control in electric furnaces: Methods, applications, and challenges. J Phys: Conf Ser, 2649(1): 012032.

Cheng S, Huang CM, Pecht M. 2017. A review of lead-free solders for electronics applications. Microelectron Reliab, 75: 77-95.

Davidson J, Ringwood JV. 2017. Mathematical modelling of mooring systems for wave energy converters-A review. Energies, 10(5): 666.

Deb D, Patel R, Balas VE. 2020. A review of control-oriented bioelectrochemical mathematical models of microbial fuel cells. Processes, 8(5): 583.

Gu A, Johnson I, Goel K, Saab K, Dao T, Rudra A, Ré C. 2021. Combining recurrent, convolutional, and continuous-time models with linear state space layers. Adv neural inf process syst, 34: 572-585.

Hannan MA, Islam NN, Mohamed A, Lipu MSH, Ker PJ, Rashid MM, Shareef H. 2018. Artificial intelligent based damping controller optimization for the multi-machine power system: A review. IEEE Access, 6: 39574-39594.

Hou Z, Chi R, Gao H. 2016. An overview of dynamic-linearization-based data-driven control and applications. IEEE Trans Ind Electron, 64(5): 4076-4090.

Jamil AA, Tu WF, Ali SW, Terriche Y, Guerrero JM. 2022. Fractional-order PID controllers for temperature control: A review. Energies, 15(10): 3800.

Karamanakos P, Liegmann E, Geyer T, Kennel R. 2020. Model predictive control of power electronic systems: Methods, results, and challenges. IEEE Open J Ind Appl, 1: 95-114.

Lashab A, Sera D, Guerrero JM, Mathe L, Bouzid A. 2018. Discrete model-predictive-control-based maximum power point tracking for PV systems: Overview and evaluation. IEEE Trans Power Electron, 33(8): 7273-7287.

Li S, Peissig J. 2020. Measurement of head-related transfer functions: A review. Appl Sci, 10(14): 5014.

Mihalič F, Truntič M, Hren A. 2022. Hardware-in-the-loop simulations: A historical overview of engineering challenges. Electronics, 11(15): 2462.

Minchala-Avila LI, Garza-Castañón LE, Vargas-Martínez A, Zhang Y. 2015. A review of optimal control techniques applied to the energy management and control of microgrids. Procedia Comp Sci, 52, 780-787.

Nise NS. 2020. Control systems engineering. John Wiley Sons, pp: 2-17.

Said M, Salleh NA, Nazeri MFM, Akbulut H, Kheawhom S, Mohamad AA. 2023. Microwave hybrid heating for lead-free solder: A review. J Mater Res Tech, 26: 6220-6243.

Silvas E, Hofman T, Murgovski N, Etman LP, Steinbuch M. 2016. Review of optimization strategies for system-level design in hybrid electric vehicles. Trans Vehic Technol, 66(1): 57-70.

Susanto T, Setiawan MB, Jayadi A, Rossi, F, Hamdhi A, Sembiring JP. 2021. Application of unmanned aircraft PID control system for roll, pitch and yaw stability on fixed wings. Int Conf Comp Sci, Inf Techn Electric Eng, October 27-28, Banyuwangi, Indonesia, pp: 186-190.

Tsui CC. 2022. Robust control system design: advanced state space techniques. CRC Press, pp: 7.

Yanarateş C, Zhou Z, Altan A. 2024. Investigating the impact of discretization techniques on real-time digital control of DC-DC boost converters: A comprehensive analysis. Heliyon, 10(20): e39591.

Zia MF, Nasir M, Elbouchikhi E, Benbouzid M, Vasquez JC, Guerrero JM. 2022. Energy management system for a hybrid PV-wind-tidal-battery-based islanded DC microgrid: Modeling and experimental validation. Renewable Sustainable Energy Rev, 159: 112093.